Protonation-driven structural deformation in conformationally twisted pyridyl-linked AIEgen: Platform to detect polyamines and nicotine

Madhuparna Chakraborty, Avanigadda Madhu Niharika, Zubair Khalid Baig, and Manab Chakravarty*

Department of Chemistry, Birla Institute of Technology and Science-Pilani, Hyderabad Campus, Hyderabad-500078, India.
E-mail: manab@hyderabad.bits-pilani.ac.in

Contents:

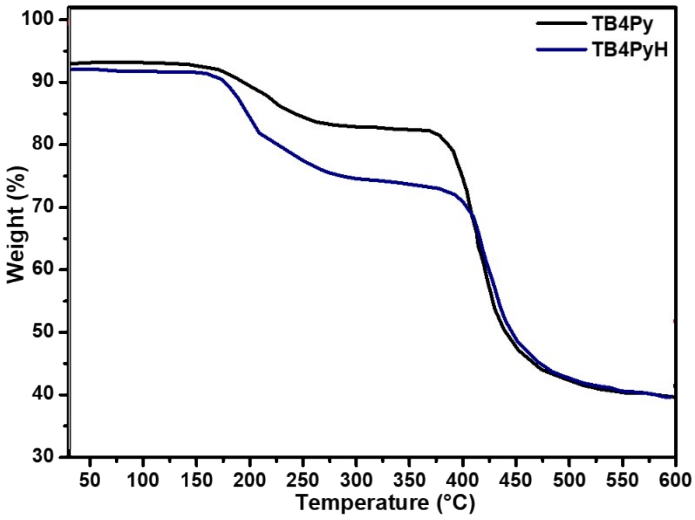

Figure S1: TGA thermogram for **TB4Py** and **TB4PyH**

Table S1: Variation in absorbance and emission with different polar solvents.

Solvents	TB4Py [$\lambda_{ex/em}$(nm)]
Hexane	404/ 485
CCl_4	409/ 495
Toluene	408/ 494
1,4-Dioxane	407/ 498
THF	407/ 492
$CHCl_3$	409/ 434, 492
CH_2Cl_2	409/ 434, 495
MeCN	405/496

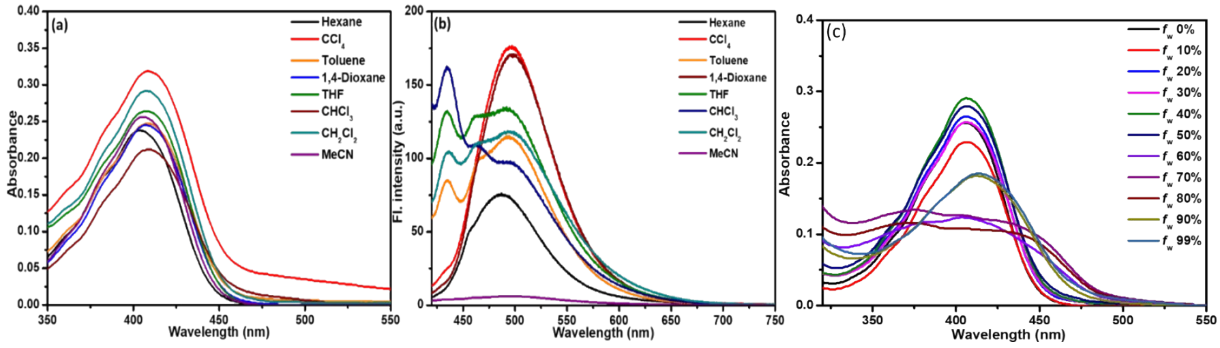

Figure S2: (a) Absorbance and (b) Fluorescence (FL) spectra of **TB4Py** (10 µM) with different solvents of a wide range of polarity [λ_{ex} = 404 - 410 nm]. (c) Absorbance spectra in AIE studies. The concentration of the probe is 10 µM in acetonitrile, and a gradual increment of water fraction (f_w).

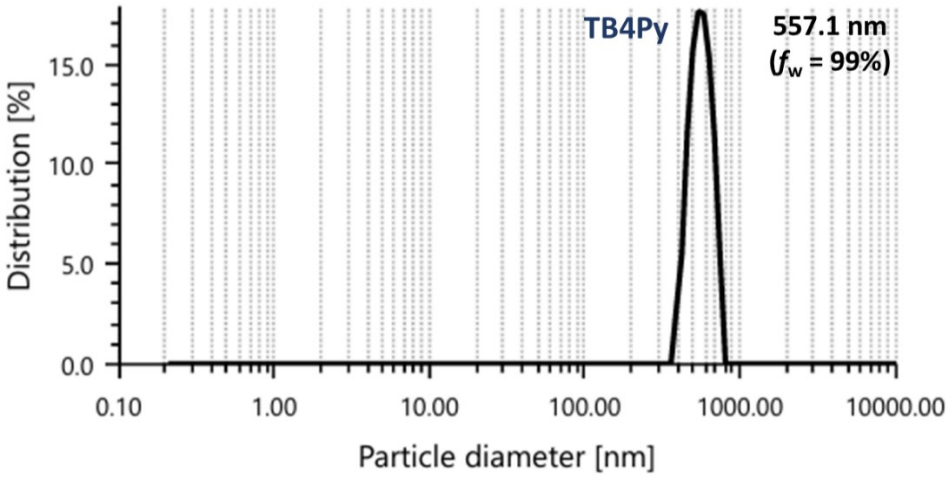

Figure S3: Average particle size distribution determination through DLS measurement studies of **TB4Py** at f_w ~ 99%.

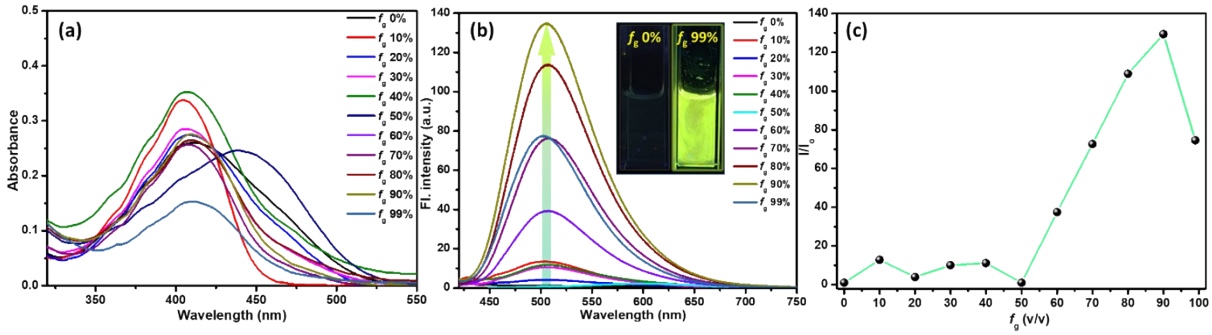

Figure S4: (a) Absorbance, (b) Emission spectra of **TB4Py**, λ_{ex} = 406 nm and (c) I/I_0 plot [I_0: Fl. intensity before the addition of glycerol, I: Fl. intensity after the addition of glycerol. The concentration of the probe is 10 µM. Inset: The image was taken at f_w = 0%, and f_w = 90% for TB4Py under 365 nm UV lamp.

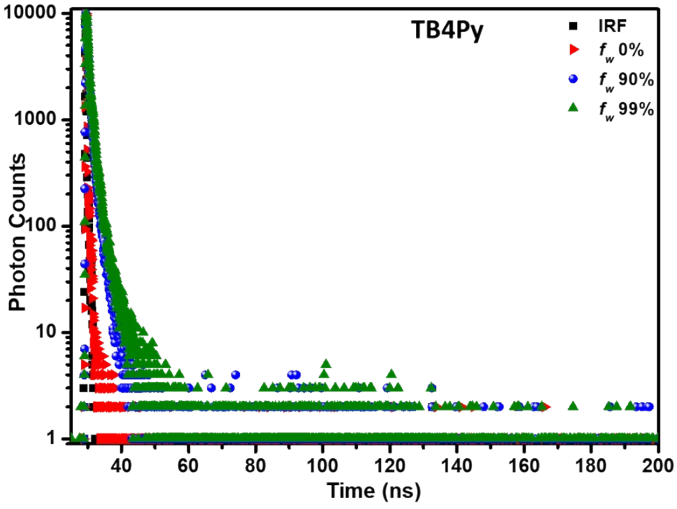

Figure S5: Time-resolved FL decay of **TB4Py** at different water fractions where the emission could be measured.

Table S2: Parameter related to lifetime (τ ; ns) measurement of excited state. λ_{ex}= 405 nm

TB4Py	α_1	α_2	τ_1	τ_2	$<\tau>$	χ^2
f_w 0%	0.99	-0.004	0.032	0.124	0.032	0.92
f_w 90%	0.90	0.098	0.46	1.73	0.58	1.07
f_w 99%	0.88	0.11	0.49	1.99	0.66	1.01

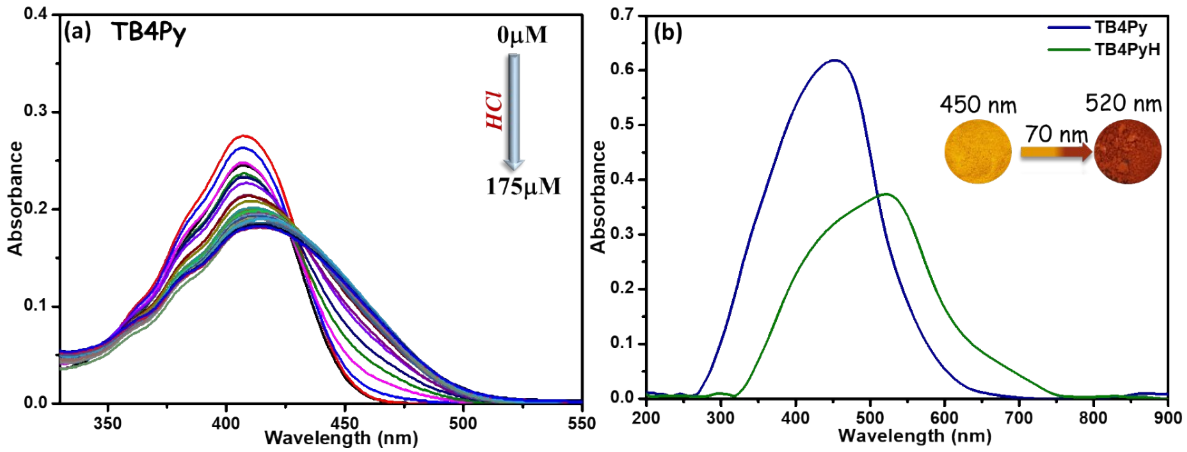

Figure S6: Absorbance of (a) **TB4Py** (10 μM in 1,4-dioxane) in solution state upon gradual addition of 10^{-2} M HCl (λ_{ex} = 407 nm) and (b) in the solid state before and after exposure to 50 μL of HCl vapor for 30 min. All the images were taken under a 365 nm UV lamp.

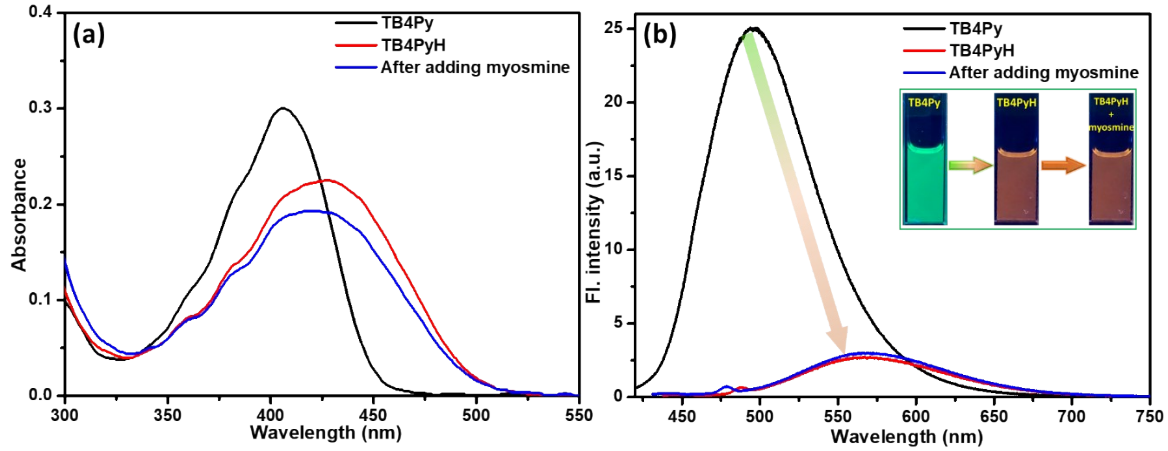

Figure S7: (a) Absorbance and (b) emission of **TB4Py** (10 μM in 1,4-dioxane) in solution state after the addition of myosmine (1mM).

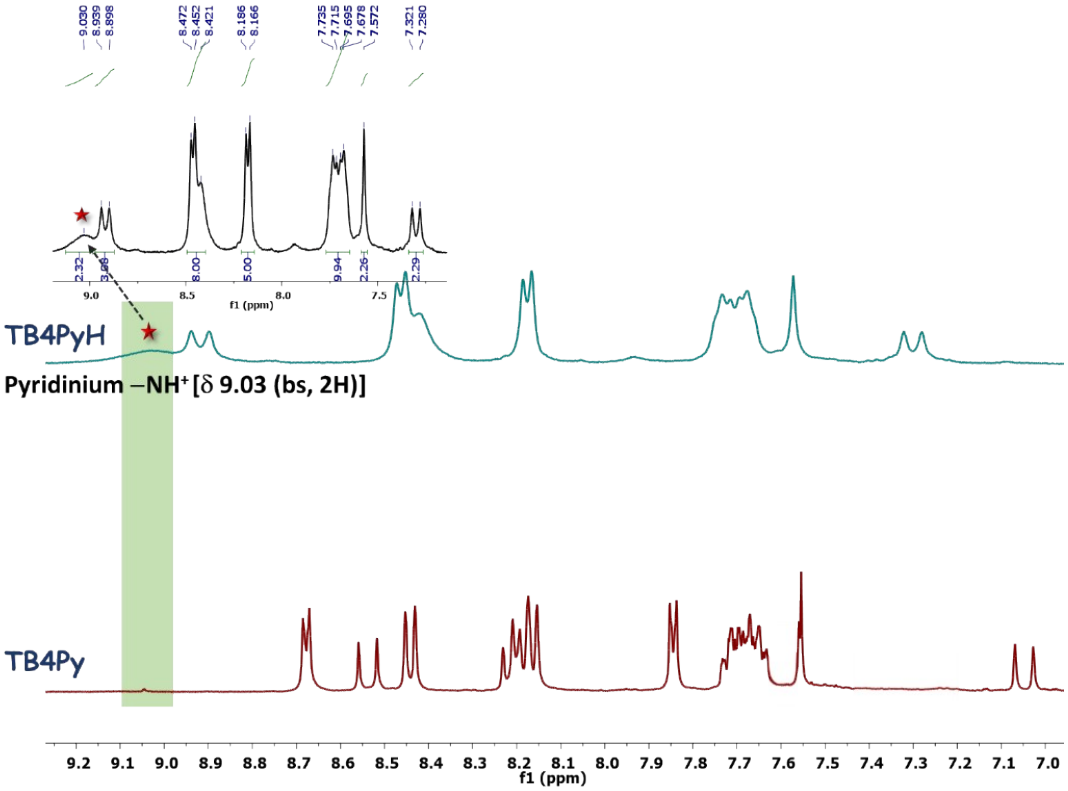

Figure S8: ^{1}H NMR spectra of **TB4Py** before and after protonation in DMSO-d_6

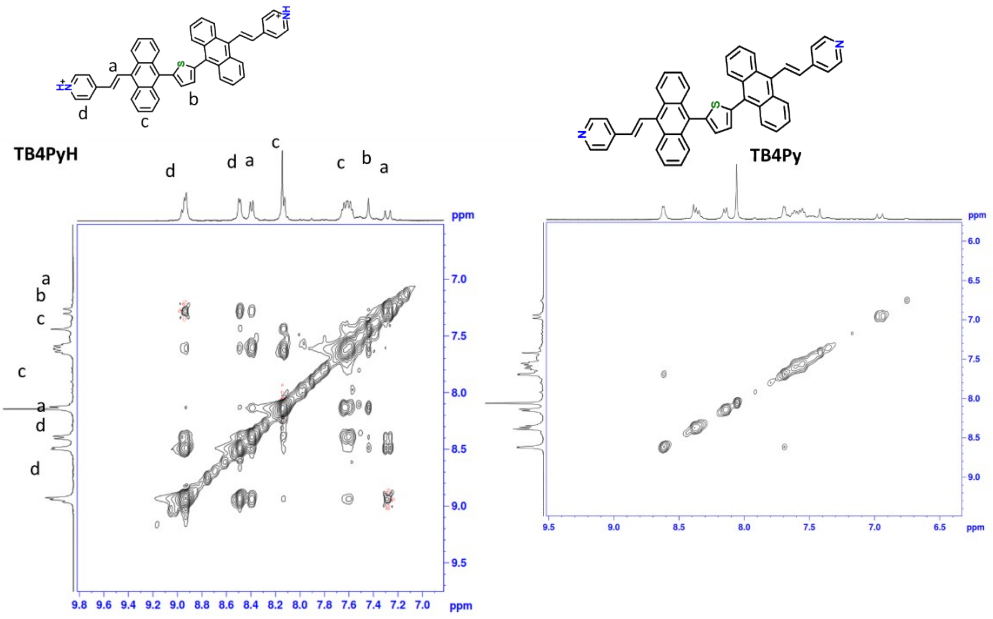

Figure S8a: The NOESY spectrum of **TB4PyH** (left) and **TB4Py** (right)

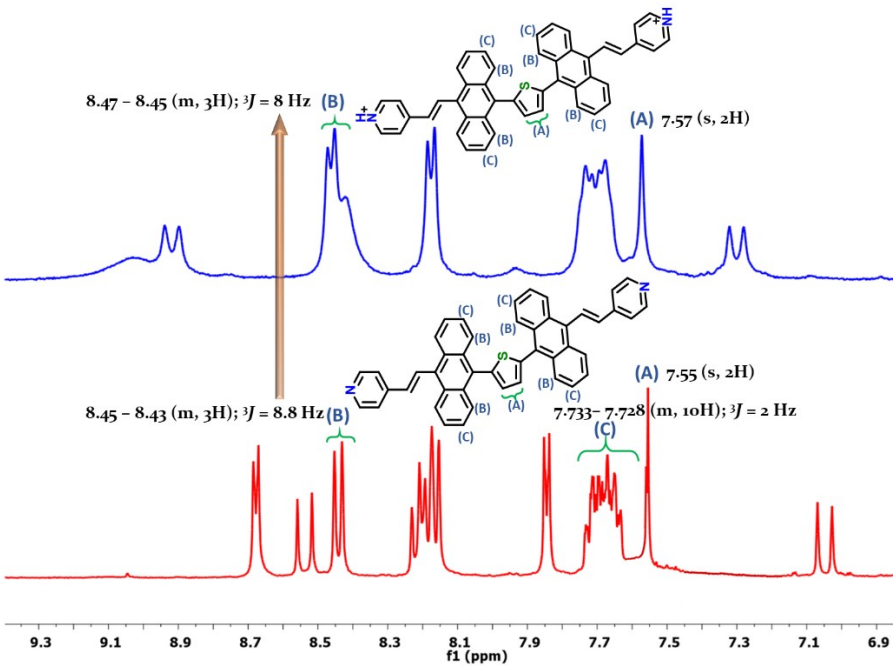

Figure S8b: The ^{1}H-NMR (400 MHz) spectra (partial) of **TB4PyH** (top; DMSO-d_6.) and **TB4Py** (down; $CDCl_3$)

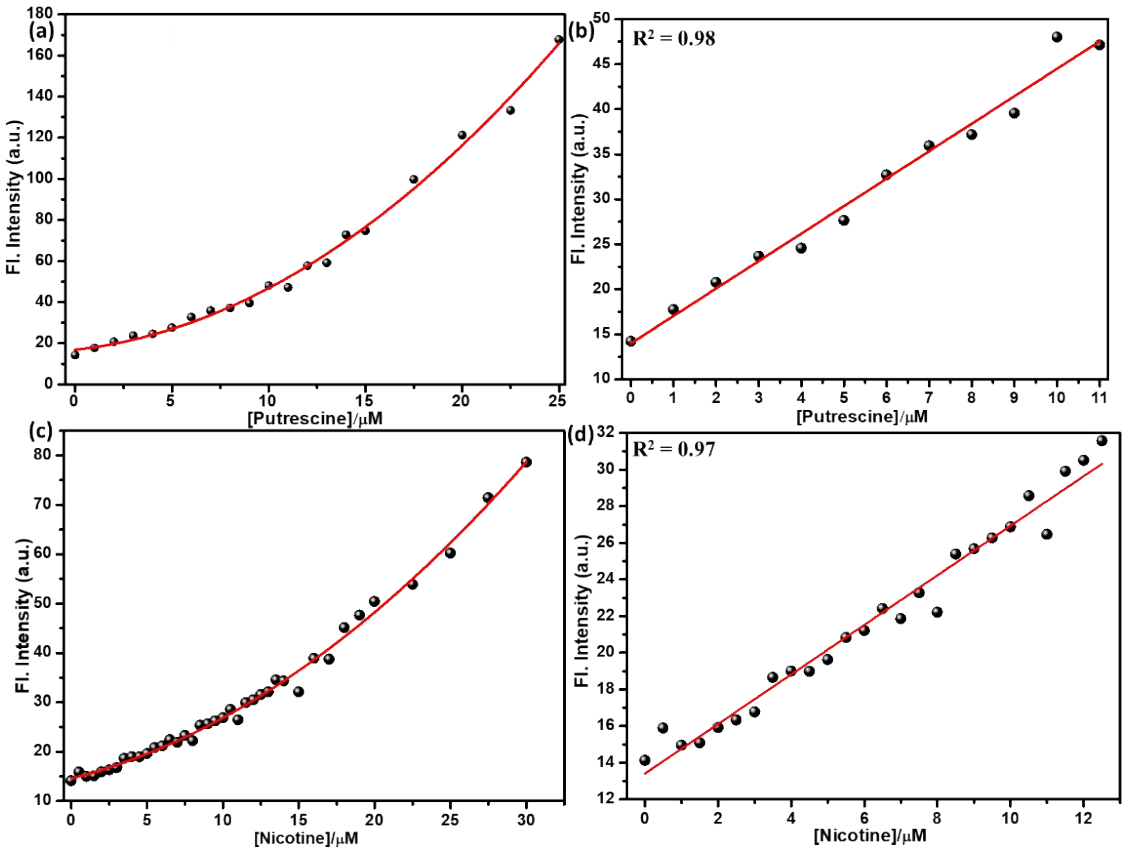

Figure S9: Limit of detection (LOD) plot for **TB4PyH** after gradually adding (a-b) Putrescine, and (c-d) NIC. [b & d are LOD plots at lower concentrations of the respective analytes)

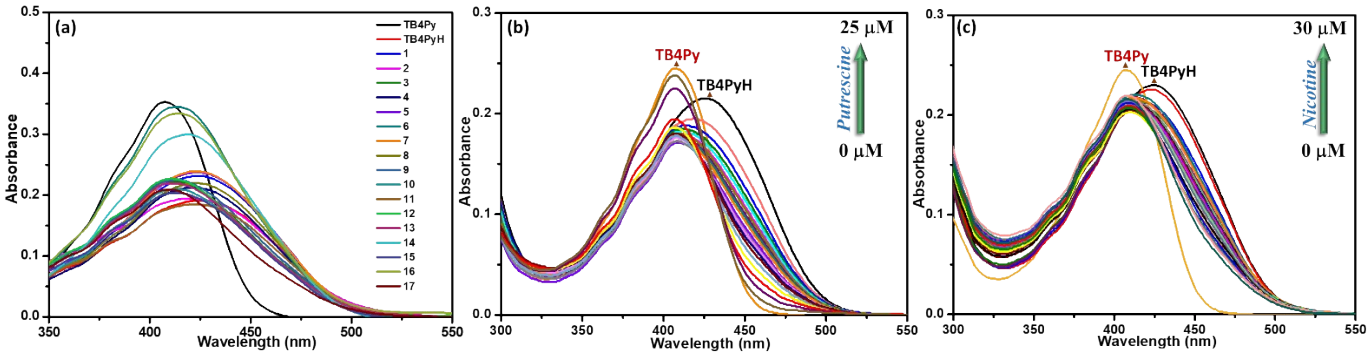

Figure S10: Absorbance of (a) **TB4PyH** (10 μM in 1,4-dioxane) after the addition of various biogenic amines (1 mM in DMAc)/ nicotine (1 mM in water) in the solution state; 1- Ammonia; 2- Butylamine; 3- Aniline; 4-Triphenylamine; 5- Diphenylamine; 6- Ethylenediamine; 7- Triethylamine; 8- 2-phenylethylamine; 9- Tryptamine; 10- N-ethyldiisopropylamine; 11- 1,3-diaminopropane; 12- Putrescine; 13- Cadaverine; 14- 1,6-diaminohexane; 15- Spermidine; 16- Spermine; 17- Nicotine; [λ_{ex} = 407 - 420 nm]; **TB4PyH** [10 μM in 1,4-Dioxane] after gradual addition of (b) PUT (1mM); [λ_{ex} = 406 nm] (c) NIC (1mM), with different volumes (in μL); λ_{ex} = 411 - 418 nm.

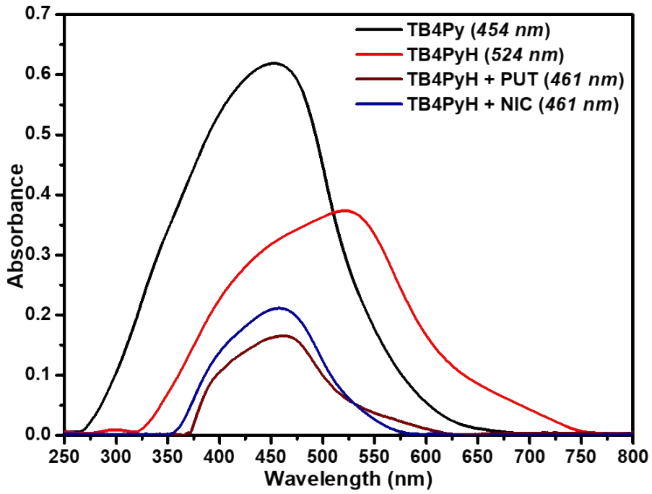

Figure S11: Solid state absorbance spectra of **TB4Py**, **TB4PyH**, **TB4PyH + PUT** and **TB4Py + NIC**.

Table S3: Variation in emission maxima, emission shift and absolute Φ_f(%) after the addition of different amine in the solid state.

Entry	Amine vapors	λ_{em} (nm)	$\Delta\lambda$ (nm)	Φ_f(%)	Amount of amine (mg/L) used inside the chamber
1	-	611	-	0.10	-
2	NH_3	548	74	1.07	109.5

3	$nBuNH_2$	528	94	2.12	111
4	EDA	526	96	3.34	134.85
5	DAP	523	99	3.17	132
6	PUT	526	96	3.25	131.55
7	CAD	523	99	3.77	130.5
8	1,6-DAH	525	97	3.52	126
9	PEA	568	43	2.80	144.3
10	DIPEA	562	60	1.90	113.5
11	Spermidine	523	99	1.81	138.75
12	Spermine	528	94	0.97	140.5

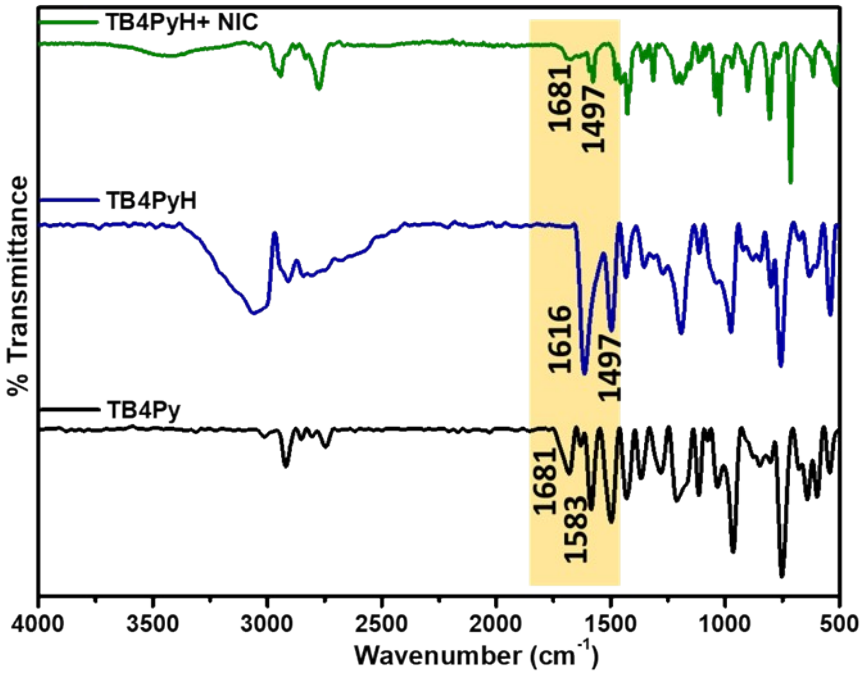

Figure S12: FT-IR spectra of **TB4Py** before and after the addition of HCl and NIC

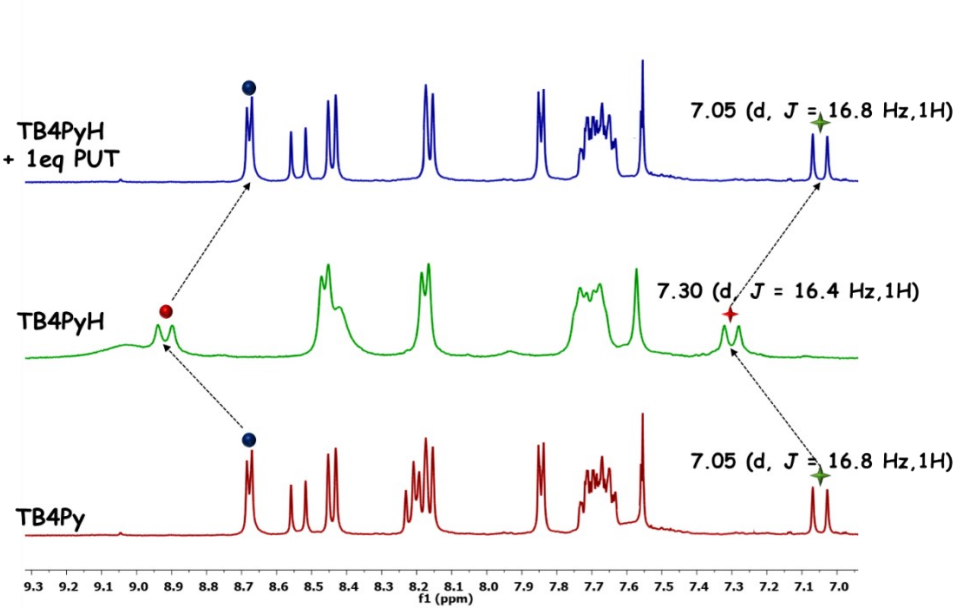

Figure S13: A partial ^{1}H NMR spectra (only aromatic part) of **TB4Py**, **TB4PyH**, **TB4PyH** +PUT (1 equiv) in DMSO d_6.

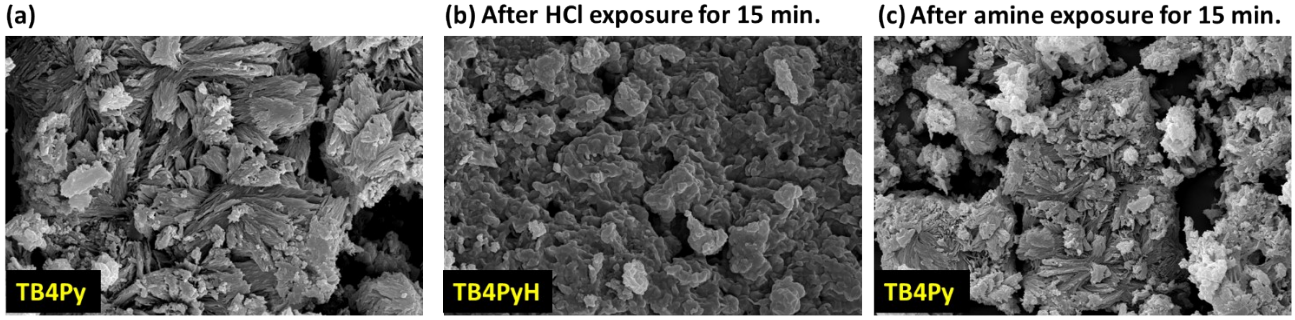

Figure S14: SEM images of **TB4Py** before and after HCl and amine vapor exposure. All the images were captured on a 5 μm scale.

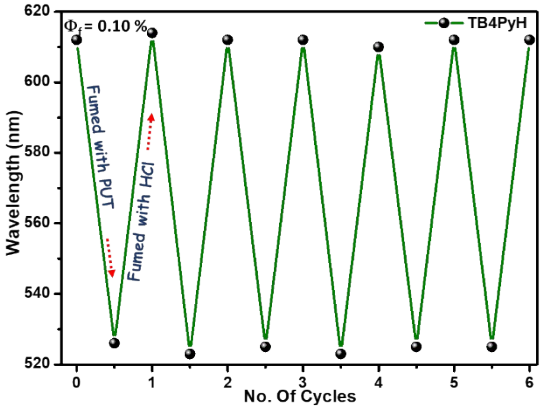

Figure S15: Reversibility plot of **TB4PyH** with putrescine (**PUT**) and HCl vapor (the Φ_f % after the 6th cycle was negligible).

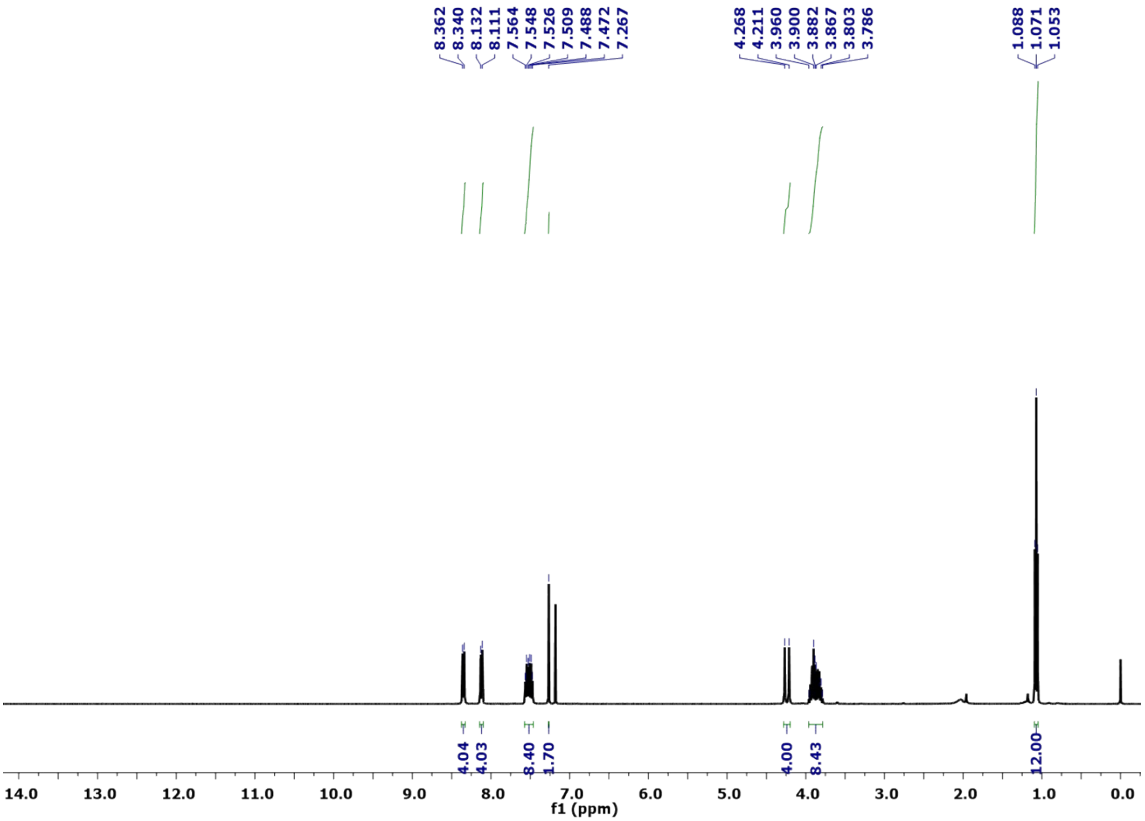

Figure S16: ^{1}H-NMR spectrum of **TBP** in $CDCl_3$.

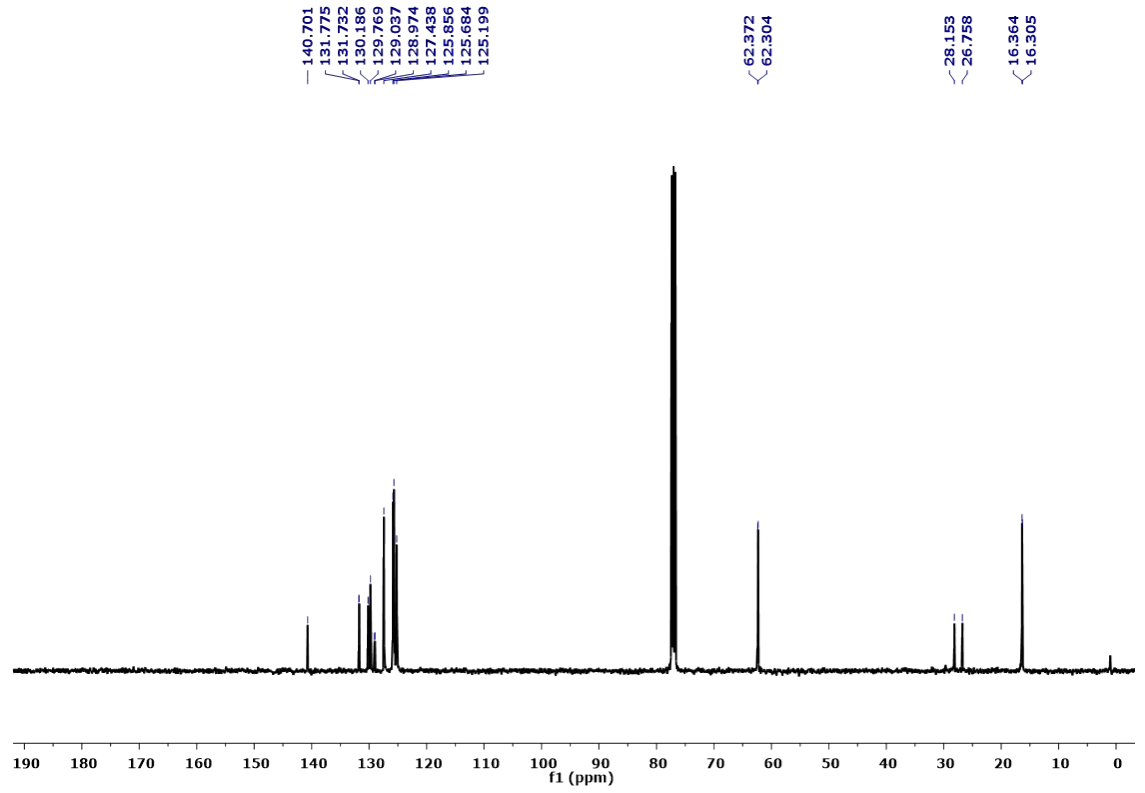

Figure S17: ^{13}C-NMR (101 MHz) spectrum of **TBP** in $CDCl_3$.

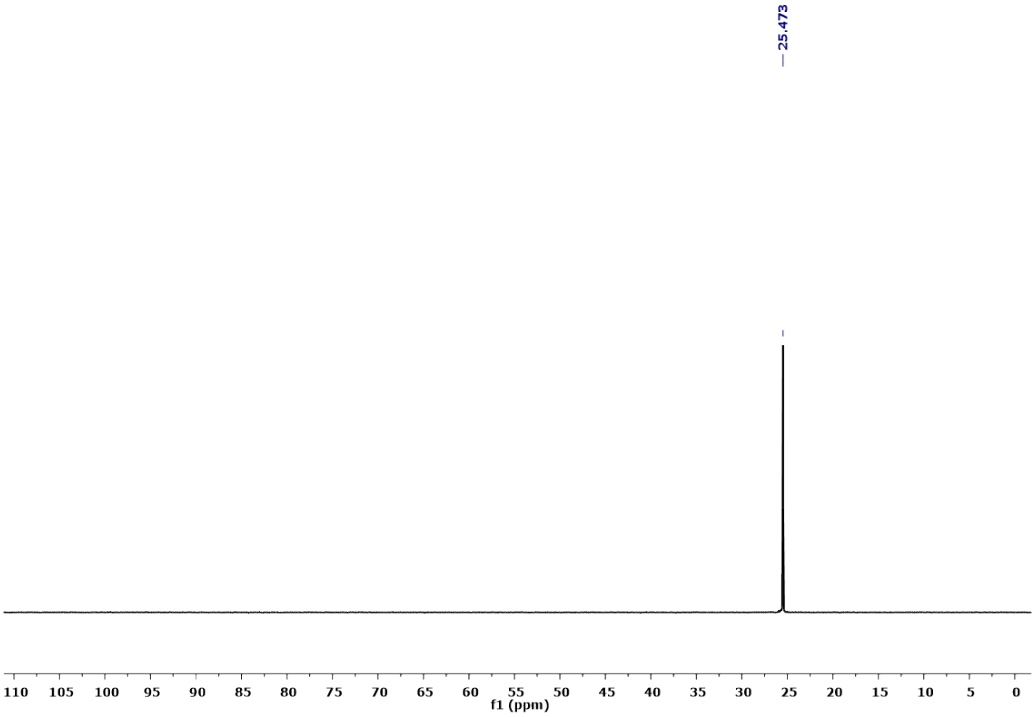

Figure S18: ^{31}P-NMR spectrum of **TBP** in $CDCl_3$.

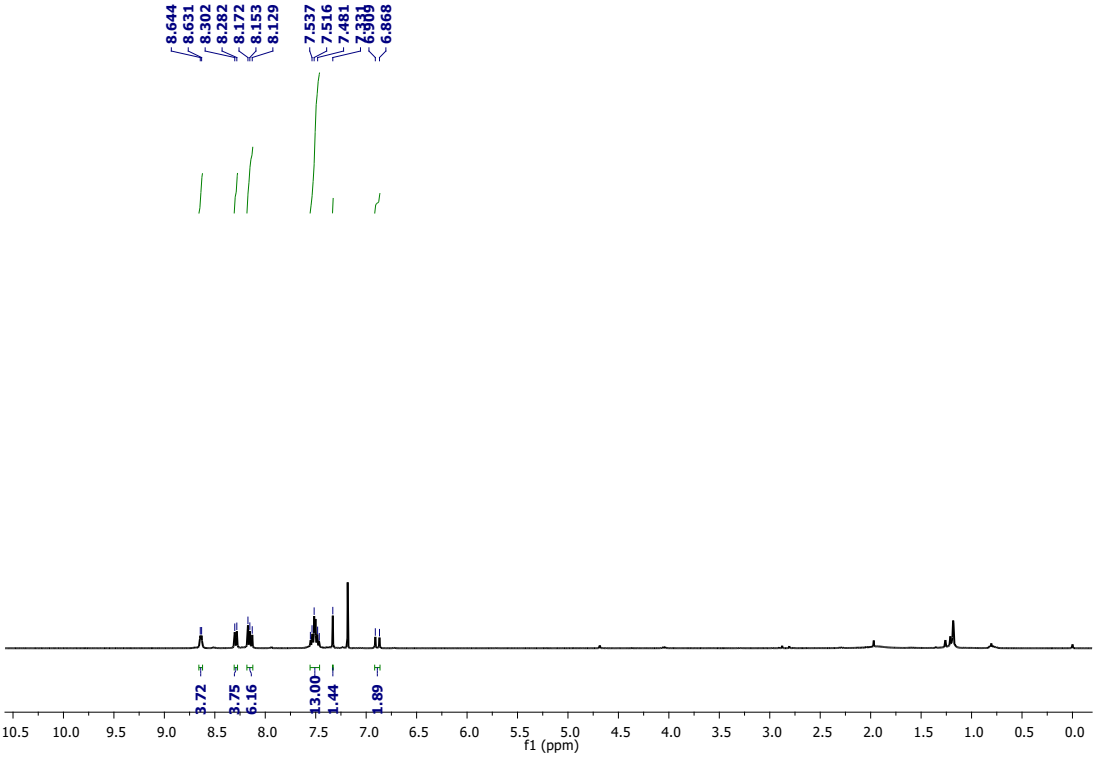

Figure S19: ^{1}H-NMR spectrum of **TB4Py** in $CDCl_3$.

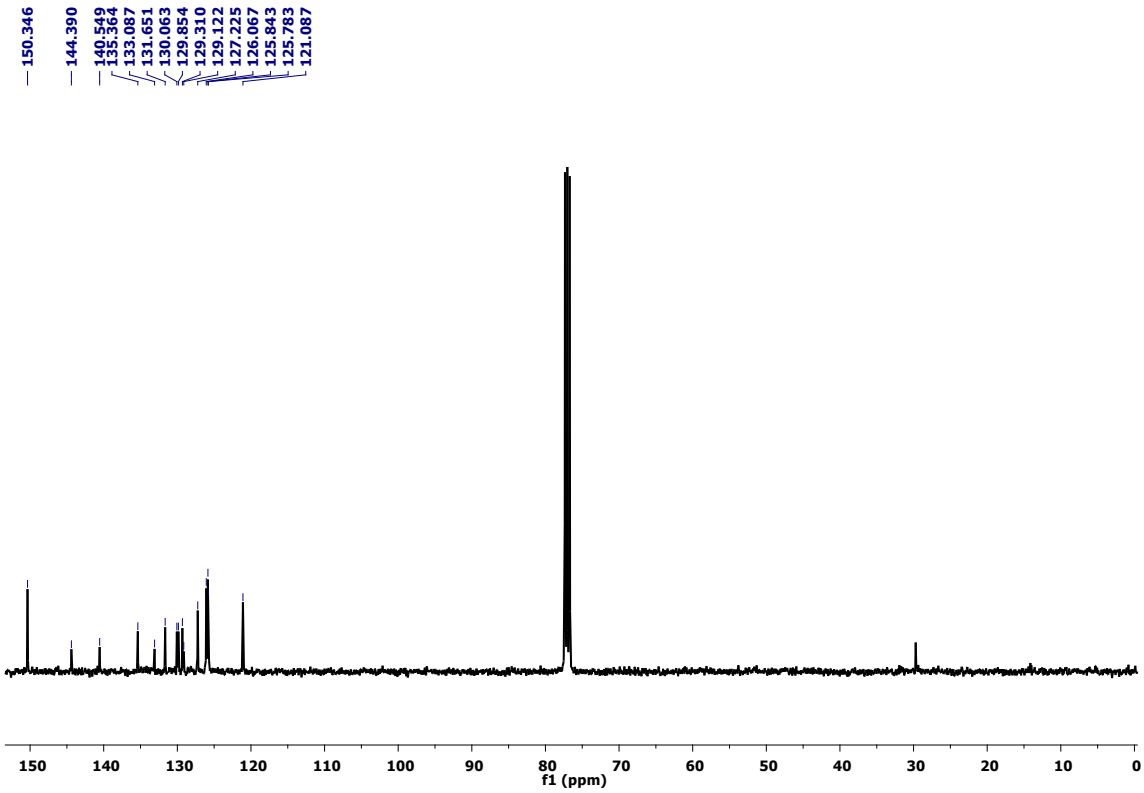

Figure S20: ^{13}C-NMR spectrum of **TB4Py** in $CDCl_3$.

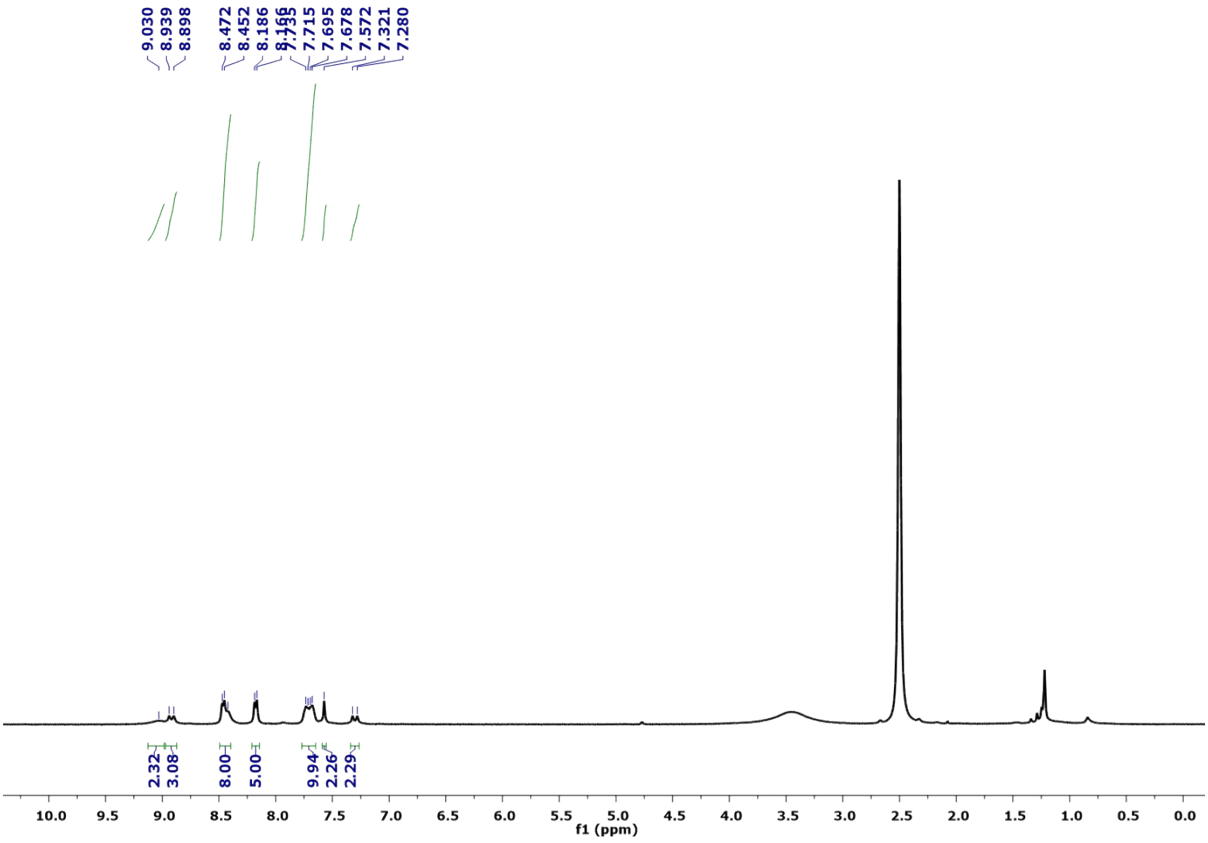

Figure S21: ^{1}H-NMR spectrum of **TB4PyH** in DMSO-d_6.

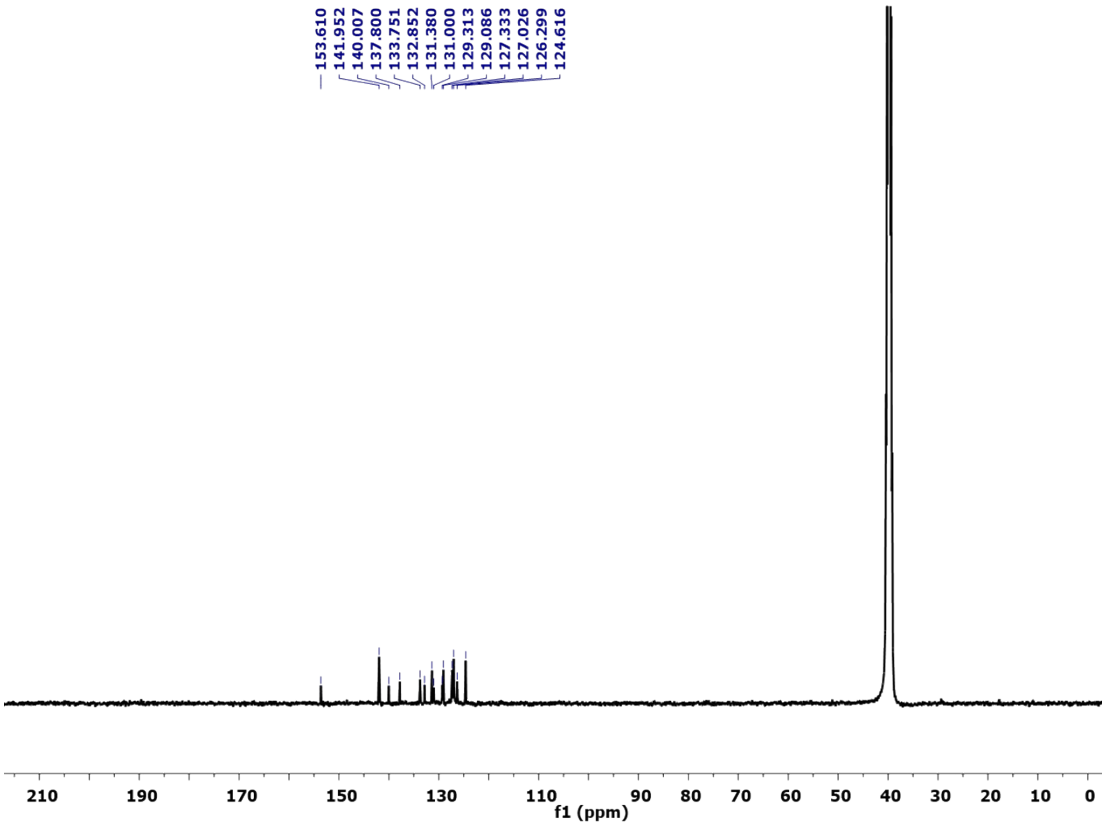

Figure S22: ^{13}C-NMR spectrum of **TB4PyH** in DMSO-d_6.

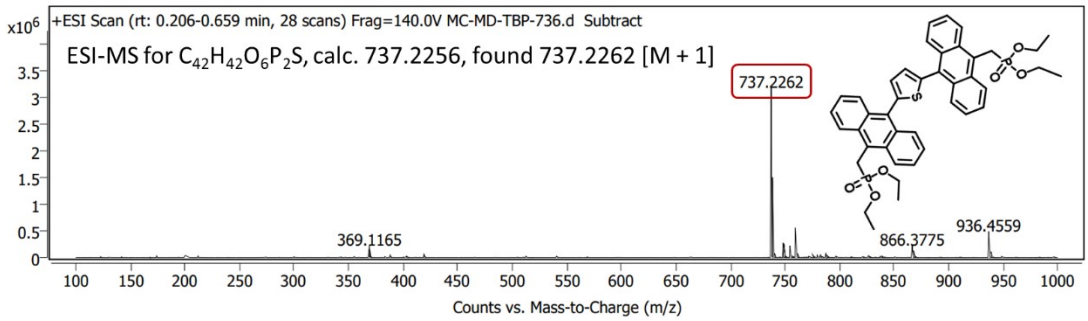

Figure S23: HR-MS spectra of **TBP**.

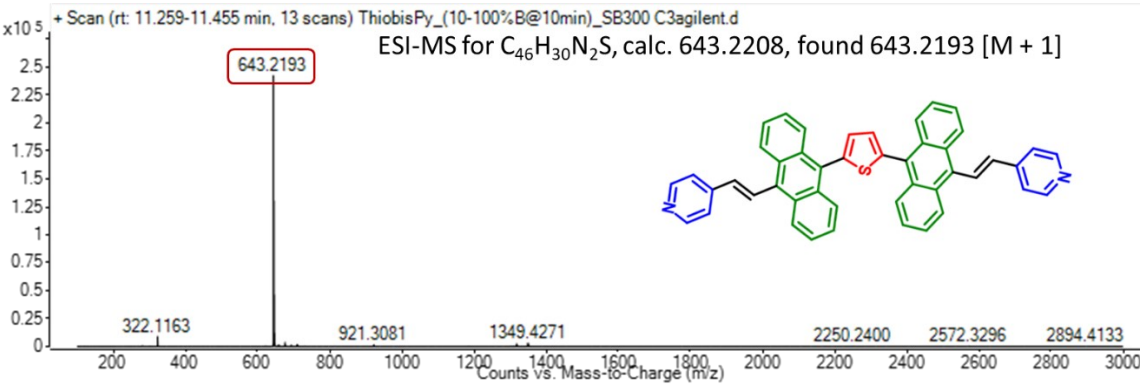

Figure S24: HR-MS spectra of **TB4Py**.

Table S4: Single-crystal X-ray parameters

Compounds	TBP
Emp. Formula	$C_{42}H_{42}O_6P_2S$
Formula Weight	736.2177
Crystal System	Triclinic
Space Group	P-1
a /Å	9.7161(3)
b /Å	13.5833(4)
c /Å	14.4482(5)
α/degree	75.704
β/degree	79.476
γ/degree	82.086
V /Å^3	1808.10(10)
Z	2
D_{calc} /g cm-3	1.3533
μ /mm^{-1}	0.227
F (000)	777
Data/ restraints/ parameters	8377/0/4655
S	1.023
R1 [I>2σ(I)]	0.0491
wR2 [all data]	0.1387
Max./min. residual electron dens. [eÅ^{-3}]	1.07/-0.59

Theoretical study and computational details:

Geometry optimizations of all the compounds are carried out with the aid of Density functional theory (DFT) using CAMB3-LYP exchange-correlation functional and 6-31G(d) basis set as implemented in Gaussian 16 suite of programs.[1]

References:

(1) Gaussian 09, Revision D.01, M. J. Frisch, G. W. Trucks, H. B. Schlegel, G. E. Scuseria, M. A. Robb, J. R. Cheeseman, G. Scalmani, V. Barone, B. Mennucci, G. A. Petersson, H. Nakatsuji, M. Caricato, X. Li, H. P. Hratchian, A. F. Izmaylov, J. Bloino, G. Zheng, J. L. Sonnenberg, M. Hada, M. Ehara, K. Toyota, R. Fukuda, J. Hasegawa, M. Ishida, T. Nakajima,

Y. Honda, O. Kitao, H. Nakai, T. Vreven, J. A. Montgomery, Jr., J. E. Peralta, F. Ogliaro, M. Bearpark, J. J. Heyd, E. Brothers, K. N. Kudin, V. N. Staroverov, T. Keith, R. Kobayashi, J. Normand, K. Raghavachari, A. Rendell, J. C. Burant, S. S. Iyengar, J. Tomasi, M. Cossi, N. Rega, J. M. Millam, M. Klene, J. E. Knox, J. B. Cross, V. Bakken, C. Adamo, J. Jaramillo, R. Gomperts, R. E. Stratmann, O. Yazyev, A. J. Austin, R. Cammi, C. Pomelli, J. W. Ochterski, R. L. Martin, K. Morokuma, V. G. Zakrzewski, G. A. Voth, P. Salvador, J. J. Dannenberg, S. Dapprich, A. D. Daniels, O. Farkas, J. B. Foresman, J. V. Ortiz, J. Cioslowski, and D. J. Fox, Gaussian, Inc., Wallingford CT, 2013.